Determination of the Cooper-pair mass in niobium

J. Tate,* S. B. Felch,† and B. Cabrera
Department of Physics, Stanford University, Stanford, California 94305-4060
(Received 7 August 1989; revised manuscript received 31 May 1990)

We have measured the ratio of Planck's constant h to the observable mass m' of a Cooper pair in a superconductor, using a rotating superconducting ring. The flux through such a ring of area S is zero for a set of rotation frequencies evenly spaced by $\Delta\nu$ and $h/2\pi m'=2S\Delta\nu$. Our measurements of S and $\Delta\nu$ enable us to quote a value of $m'/2m_e$ for niobium of 1.000 084(21). This result disagrees with predictions from currently available theories.

I. INTRODUCTION

This paper presents the results of an experiment to measure the mass of a Cooper pair of electrons in a superconductor to an accuracy approaching the part-per-million (ppm) level. It was London[1] who first predicted that a superconductor, rotating at angular velocity ω, should have a uniform magnetic field throughout its interior given by $\mathbf{B}_L=-(2m^*c/e^*)\omega$, where e^* is the charge of the supercurrent carriers (<0) and m^* their mass. His prediction has been verified experimentally to a few percent,[2] and at this level is consistent with $e^*=2e$ ($e<0$) and $m^*=2m_e$, with m_e the free-electron mass. Much higher precision measurements of the mass are possible by determining the London flux through a rotating ring in terms of an area S and the flux quantum $\phi_0=hc/|e^*|$ as first reported by Zimmerman and Mercereau,[3] later by Parker and Simmonds,[4] and most recently by our group.[5,6] Unlike the flux quantum ϕ_0, which is Lorentz invariant, the mass appearing in the London magnetic field contains relativistic corrections and is expected to differ from twice the free-electron mass $2m_e$.[7-11] The measured mass is expected to be about 8 ppm smaller than $2m_e$ for niobiuim.[11] Our experiment measured a mass 84 ppm larger than $2m_e$ with an accuracy of 21 ppm. This error is dominated by systematic effects, and the statistical error of 5 ppm is small in comparison. In Sec. II we describe the present theory relating to the relativistic corrections and outline our experiment in terms of the Ginzburg-Landau theory. Section III deals with the experimental realization of the measurement of the London moment flux in terms of the flux quantum using a rotating thin-film ring. The results and the all-important discussion of systematic errors are contained in Sec. IV and some prospects for improving the precision are discussed in Sec. V.

II. THEORY

There have been a number of theoretical discussions in the literature which address the question of the Cooper-pair mass.[7-11] Here we summarize the approach of Cabrera and Peskin which we believe reconciles previous theoretical discrepancies (see discussions in Ref. 11). The Cooper-pair mass parameter m^* is defined as the proportionality constant between the velocity $\mathbf{v}$ and momentum $m^*\mathbf{v}=(h/2\pi)\nabla\varphi-(e^*/c)\mathbf{A}$, where φ is the phase of the macroscopic and coherent order parameter and $\mathbf{A}$ is the magnetic vector potential. Deviations from $2m_e$ arise from two sources. First, the mass of the composite Cooper pair contains a large kinetic-energy term such that m^* is greater than $2m_e$ by about 180 ppm for niobium (on this scale the binding energy of a Cooper pair is negligible). We call this mass m^* the intrinsic Cooper mass. Second, there is a contribution to the magnetic vector potential $\mathbf{A}$ within the superconductor which arises from the motion of the internal electrostatic potential in the laboratory frame. Since this contribution to $\mathbf{A}$ cannot be observed from outside of the metal, it is convenient to define an observable mass m' such that

$$m^*\mathbf{v}+(e^*/c)\mathbf{A}=m'\mathbf{v}+(e^*/c)\mathbf{A}_{\rm obs}\ ,$$

where now $\mathbf{A}_{\rm obs}$ contains only contributions from currents and can be measured outside the superconductor, and $\mathbf{A}=\mathbf{A}_{\rm obs}+(\mathbf{v}/c)\langle\Phi\rangle$, where $\langle\Phi\rangle$ is an averaged value of the electrostatic potential in the lattice.[9,11] This second correction is slightly greater than the first in magnitude and of opposite sign so that it is predicted that m' is less than $2m_e$ by ~ 8 ppm for niobium. In this paper, we report on an experimental determination of m' of sufficient accuracy to probe the relativistic regime for the first time.

To analyze our experiment, we consider flux quantization and the London moment in a rotating, superconducting ring within the framework of the Ginzburg-Landau current equation suitably modified to include the effects of rotation. We may use nonrelativistic equations because the rotation velocity $\mathbf{v}=\omega\times\mathbf{r}$ is, at most, 1 m/s. In this limit, the relativistic corrections are included in the parameter m', and the effect of rotation is kinematically equivalent to the application of a uniform magnetic field (or an additional vector potential) so that

$$(4\pi\lambda^2/c)\mathbf{j}=(hc/2\pi e^*)\nabla\varphi-\mathbf{A}_{\rm obs}-(m'c/e^*)\omega\times\mathbf{r}\ , \tag{1}$$

where λ is the London penetration depth. Integrating Eq. (1) around the ring for a closed path Γ entirely within

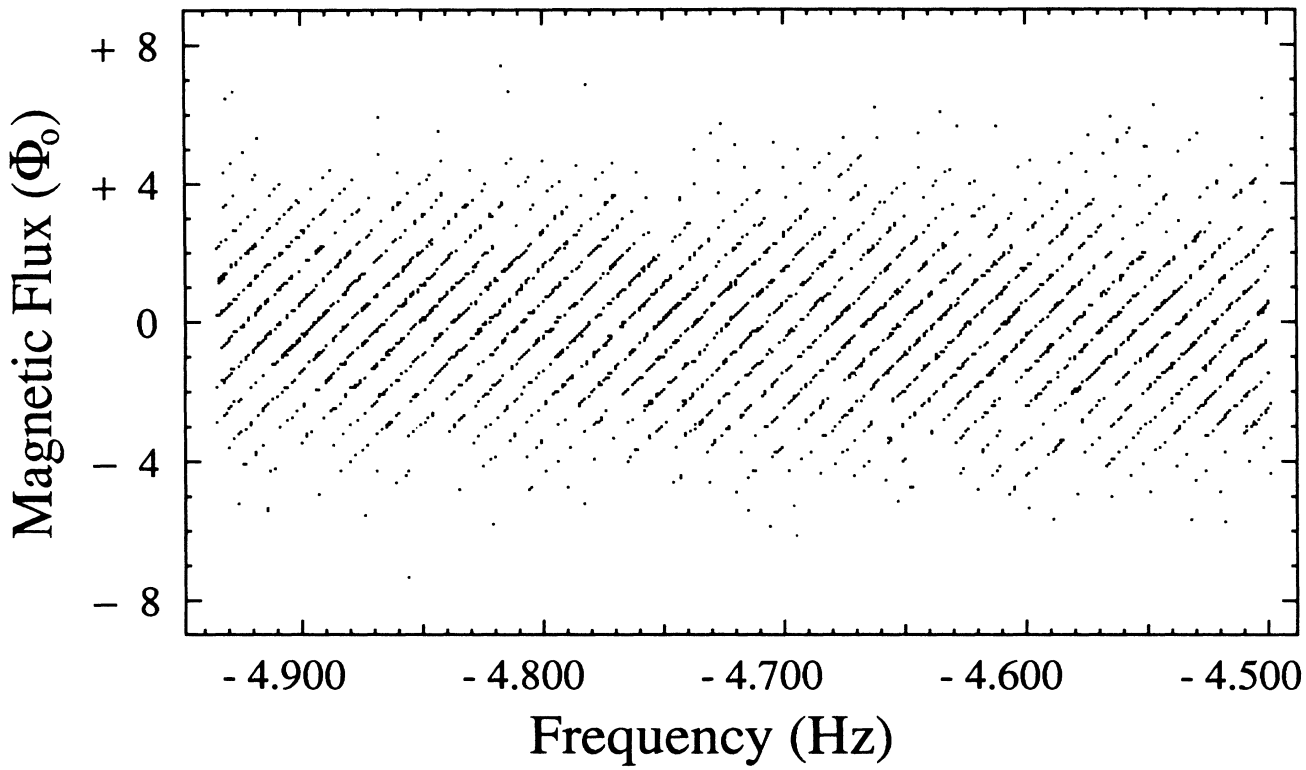

FIG. 1. SQUID output as a function of the rotation rate of the niobium ring over a 440-mHz interval.

the superconductor and requiring that the order parameter be single valued, we obtain

$$(4\pi\lambda^2/c)\int_\Gamma \mathbf{j}\cdot d\mathbf{l} = n(hc/e^*) - \phi_{\rm obs} - (2m'c/e^*)\boldsymbol{\omega}\cdot\mathbf{S}\ , \tag{2}$$

where S is the area bounded by Γ and n is an integer. This equation relates the observed flux $\phi_{\rm obs}$ through the ring to its rotation rate $\omega = 2\pi\nu$ and describes a family of parallel straight lines, one for each n. Figure 1 shows our experimental data for Eq. (2). There exists a frequency ν_n for each n such that the flux $\phi_{\rm obs}$ and j are zero together. We define this flux null spacing by $\Delta\nu \equiv \nu_n - \nu_{n-1}$ and subtract equations for n and $n-1$ to obtain

$$h/(2\pi m') = 2S\Delta\nu\ , \tag{3}$$

the primary relation used to analyze our experiment.

III. EXPERIMENT

The determination of h/m' was accomplished by measuring the flux through a thin-film superconducting niobium ring as a function of its rotation rate. The ring was deposited on the equator of a quartz rotor which was slightly larger than a hemisphere. The rotor defined the area of the ring and facilitated its rotation in a cryogenic helium-gas bearing. The technique used for the area measurement was the subject of a separate publication[12] and is only summarized here. The results of the flux null determination were summarized in an earlier publication,[6] and this paper details the experimental procedure, the data analysis, and the error sources.

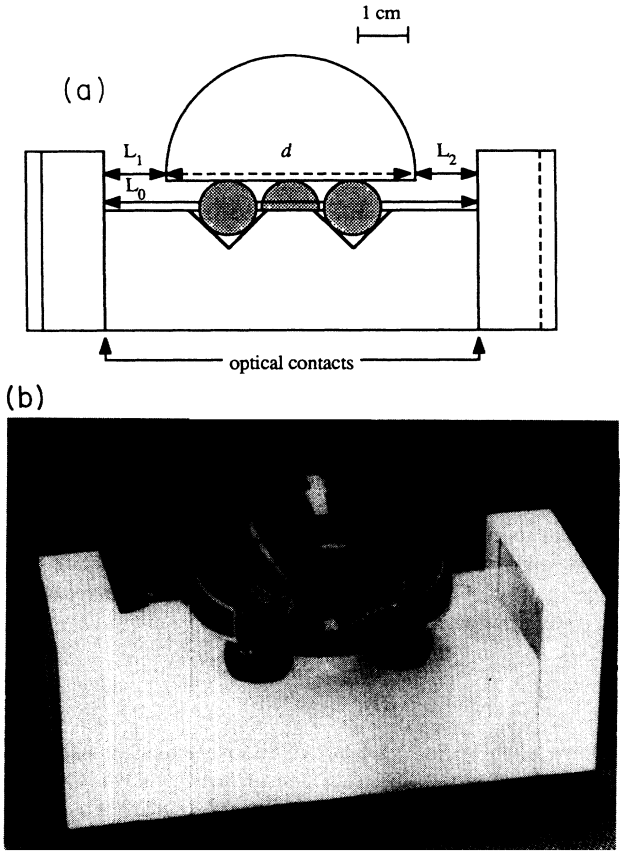

FIG. 2. (a) Schematic of the rotor in the optically contacted Fabry-Perot etalon used for the diameter determination. (b) Photograph of the apparatus.

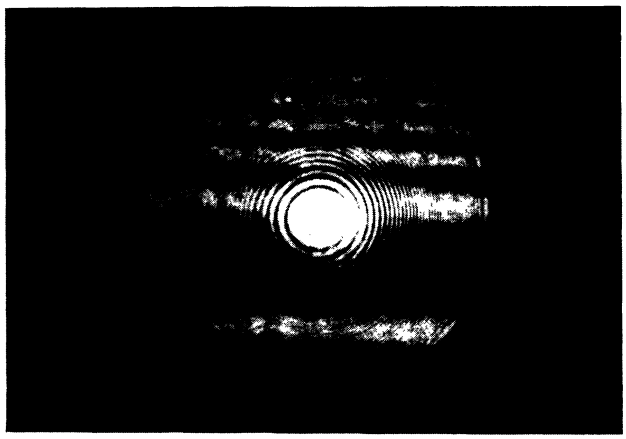

FIG. 3. Circular interference pattern produced by the laser light in one of the optical cavities in Fig. 2. The superimposed parallel line diffraction pattern is from the niobium ring.

A. Area measurement

The cross-sectional area of the thin-film niobium ring was obtained from measurements of two perpendicular diameters of the rotor at 6 K and a roundness measurement at room temperature. We also measured the same diameters at room temperature, confirming previous measurements by the National Bureau of Standards.[13] We found that the area of the ring at 6 K was 20.235 057(179) cm^2. This number includes a correction for a small misalignment of the ring with respect to the rotor's equator, and the quoted error includes the finite width and thickness of the ring and the out-of-roundness of the rotor. At 6 K, the area of the rotor is 90 ppm larger than at room temperature.

We used an interferometric technique to measure the diameter of the rotor.[12] The rotor was placed inside a plane parallel, optically contacted Fabry-Perot etalon as shown in Fig. 2, and cooled to 6 K in a rarified atmosphere of helium. A tunable, single-frequency dye laser was used to produce circular interference patterns (shown in Fig. 3) from the separations L_0, L_1, and L_2. As the frequency of the laser changed, the intensity at the center of each pattern was modulated as new fringes appeared or disappeared at the center. The number of fringes N_i ($i=0,1,2$) that appeared for a given change in frequency Δf is related to the corresponding separation L_i by

$$\Delta f = N_i c/2\mu L_i \ , \tag{4}$$

where c is the speed of light in vacuum and μ is the index of refraction of the medium traversed by the light. The rotor diameter was obtained from

$$d=(N_0-N_1-N_2)c/2\mu\Delta f \equiv Nc/2\mu\Delta f \ . \tag{5}$$

We used Doppler-free saturation spectroscopy to reference the laser frequency to accurately calibrated absorption lines in each of molecular tellurium and molecular iodine, and determined Δf (approximately 34 THz) to 0.16 ppm. For our 5-cm-diam rotor, this frequency range corresponded to $N=(N_0-N_1-N_2)\approx 11\,500$. We determined the integral part of N exactly, and the fractional part to 3%, giving a total error in N of 2.6 ppm. The dominant error in the length determination came from systematic effects relating to the size of the aperture used to view the fringe patterns, giving an overall uncertainty in the cross-sectional area of the niobium ring of 8.8 ppm.

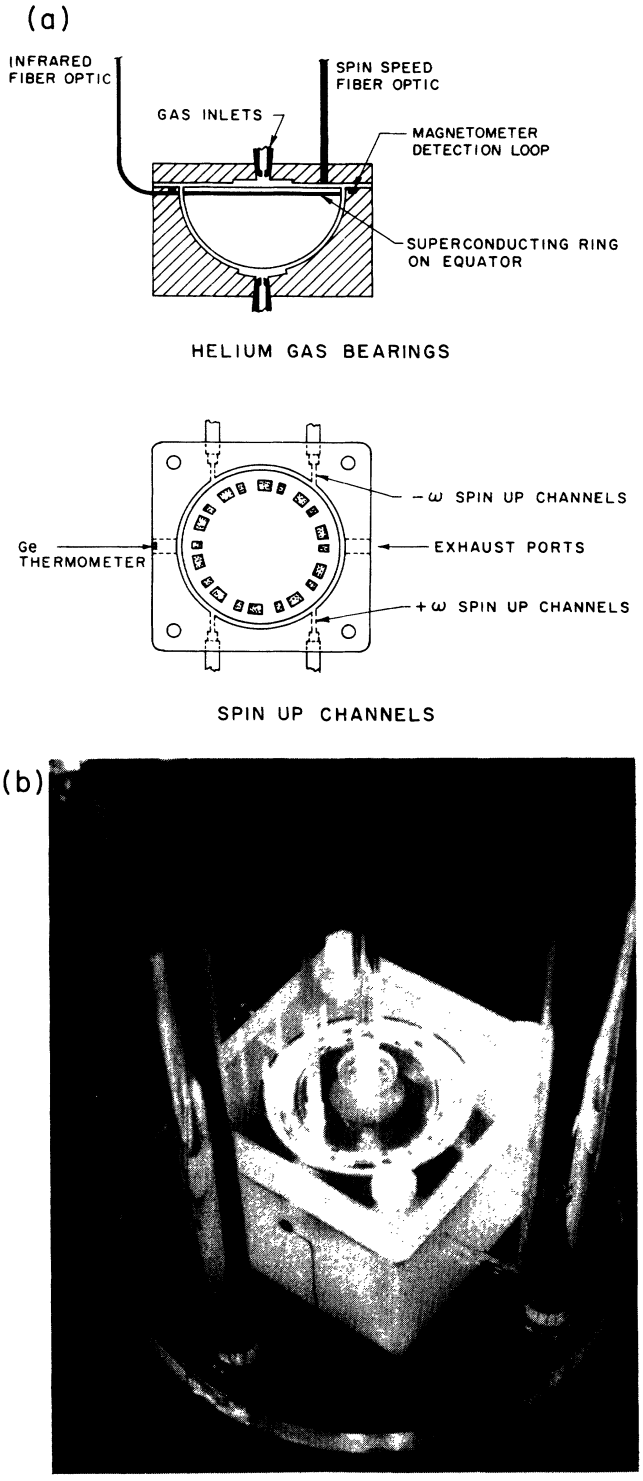

FIG. 4. (a) Schematic of the fused quartz apparatus used to determine flux null spacing. (b) Photograph of the apparatus.

B. Flux null spacing measurement

Figure 4 shows the apparatus used to measure the flux null spacing. We describe it briefly and refer the reader to Ref. 5 for details. The superconducting ring, a thin-film band of niobium, 20-μm wide and 40-nm thick, was deposited on the equator of a 5-cm-diam fused quartz rotor. The rotor was levitated and spun about its symmetry axis in a cryogenic helium-gas bearing. The position of the ring on the rotor and the tolerances in the bearing constrained the area vector and spin axis to be coincident to within a mrad. The torque to spin the rotor was provided by 99.999% pure helium gas at approximately 6 K. The maximum rotation frequency used was 5 Hz, in either direction. A frosted pattern on the rotor flat provided a signal at ten times the rotor frequency. This was used in a feedback loop to stabilize the frequency to 1 mHz. The signal was electronically divided by ten to produce a signal at the rotor frequency which was read by a frequency counter to seven-digit accuracy. A SQUID (superconducting quantum interference device) magnetometer measured the flux through the ring. The SQUID pickup loop, inductively coupled to the niobium ring, was located in a groove in the rotor housing, and remained stationary as the ring rotated. The bearing was encased in a double-walled vacuum jacket which was immersed in liquid helium. A superconducting lead shield[14] surrounded the apparatus and maintained the ambient magnetic field at 5×10^{-8} G, thus providing an adequate signal-to-noise ratio.

Typical data showing flux through the ring as a function of rotation rate are shown in Fig. 1. The prediction of Eq. (2) is clearly fulfilled, with each point in Fig. 1 assignable to a quantum state n. The spacing of the points on any line of constant frequency corresponds to a change in the flux in the ring of one flux quantum. For our system, this implies a change in magnetic field of about 10 nG, which produced a change of 11.2 mV in the SQUID output. The spacing of the points on any line of constant flux is the $\Delta\nu$ of Eq. (3) and was about 14.3 mHz. Each point in Fig. 1 is the average speed and flux over an integer number of rotations—usually two or three. Between each data point, a portion of the niobium ring was driven normal by a 100-ns burst of radiation from a 789-nm laser diode directed onto the ring via a single fiber optic. A few mW of radiation was sufficient to destroy superconductivity in a small section, thus destroying the phase coherence around the ring and allowing the magnetic field to leave or enter. Upon removal of the heat, phase coherence was reestablished after about 100 ms (the thermal time constant of the quartz rotor) and a definite quantum state accessed. The most likely quantum state is the one with the least current in the ring, and states with larger current (in either direction) are accessed with decreasing probability. In fact, the probability distribution is Gaussian, with a standard deviation given by

$$\sigma=(Lk_BT^*/\phi_0^2)^{1/2}\ , \tag{6}$$

where L is the self-inductance of the ring, k_B is the Boltzmann constant, and ϕ_0 is the superconducting flux quantum. T^* is the temperature at which the rate of thermally activated transitions between quantum states becomes unobservable, and is slightly lower than the thermodynamic transition temperature T_c. In this case, $L=0.275$ μH, which gives $T^*=6.2$ K, expected for a film of this thickness.[15]

Magnetic flux could be trapped as a vortex in the niobium film itself during the superconducting transition. In this case, the average flux measured by the SQUID was nonintegral, because the current paths in the ring above the vortex enclosed one more (or less) flux quantum than those below. Provided the same portion of the ring was driven normal each time (accomplished by triggering the heat pulse with the rotor frequency signal), any vortex trapped was likely to be released at the next heat pulse. Such events were easily identifiable in the data, and the offending point was discarded. If the flux vortex remained trapped, however, all subsequent flux measurements were displaced relative to those before the trapping by some fraction of a flux quantum. This, of course, shifted all subsequent flux nulls by some amount, introducing an error into the null spacing determination. If permanent vortex trapping was identified in the data, that data set was discarded, but if it happened while the flux was not being recorded, the only indication of the occurrence was an anomalous value of $\Delta\nu$. We will return to this point in our discussion of the data analysis.

1. *Electrostatic charging of the rotor*

Equation (3) was derived assuming that the current measured by the SQUID pickup loop is due only to the supercurrent in the niobium ring. The change in flux with rotation rate is then the London moment $(\partial\phi/\partial\omega)_{SC}$. We tested the accuracy of the assumption by heating the ring above its critical temperature and monitoring the SQUID output as the rotor spun. We measured a small change in flux with rotation rate $(\partial\phi/\partial\omega)_N$ proportional to the rotation rate, caused by an electric charge on the rotor. The parameter

$$\delta\equiv(\partial\phi/\partial\omega)_N/(\partial\phi/\partial\omega)_{SC}$$

varied between $+0.0025$ and -0.003 during different experimental runs. We calculated[5,16] the effect of a charge distribution on the flux null spacing by considering the rotor to consist of bands of current which couple to the supercurrents in the ring and the SQUID pickup loop. The result was that the flux null spacing measured in the presence of a rotor charge $\Delta\nu(\delta)$ is related to the spacing in the absence of charge $\Delta\nu(0)$ by

$$\Delta\nu(\delta)=\Delta\nu(0)(1-\epsilon\delta)\ , \tag{7}$$

or, stated in terms of the corresponding mass parameters [From Eq. (3)],

$$m'(\delta)=m'(0)(1+\epsilon\delta)\ , \tag{8}$$

where ϵ is a constant which depends on the charge distribution and the inductive coupling between the current bands. Calculation of the relevant inductances based on the geometry of the apparatus yielded a numerical estimate of $\epsilon=0.702(35)$ for a uniform charge distribution to

compare with the experimentally determined value. For any nonuniform charge distribution, ϵ deviates from this value by only a few percent as long as the surface charge density varies slowly over the small region around the niobium line (see Ref. 5 for details).

We made several attempts to reduce the charge. We introduced grounded wires and radioactive sources into the gas lines as close as possible to the rotor. We also coated the rotor with a 10-nm film of granular aluminum, and pushed it against a grounded plane before each run. It proved impossible to ground the rotor continuously. Although we were unsuccessful in eliminating the charge, these data show charge levels that are ten times lower than in the earliest runs. Within this reduced range, we managed to vary the size and sign of the charge for a range of δ values allowing a good fit to Eq. (7). The origin of the charge remains something of a mystery. In the original configuration, the charge was positive, and the value of δ led to an estimate of 10^{10} charges on the rotor, which put the rotor potential at roughly 1 kV. We estimate that, for such a potential, the gas-flow viscosity can just carry an ion against the electric force. The charge built up over a period of hours and discharged somewhat over a period of days if the rotor was not spun. We assume that helium gas flowing through teflon bellows (which were often charged negatively when the apparatus was warmed up) became positively charged and then stripped electrons from the quartz as it flowed past sharp surfaces. Once the rotor was coated with a thin metallic film, the sign of δ reversed but then gradually (over weeks) headed towards zero, and became positive again.

2. *Data acquisition*

The data acquisition was designed to exploit the predicted linear dependence of $\Delta\nu$, or equivalently m', on δ [Eqs. (7) and (8)]. The scheme is outlined in Fig. 5, which shows the magnetometer output when the ring is superconducting (quantized flux labeled "*S*") and normal ("*N*") at different rotor frequencies. With the rotor spinning at a constant frequency ν_1 and the niobium ring normal, 70 pairs of flux-frequency points were recorded. Then, with the ring superconducting at ν_1, 70 more pairs were recorded, with a small portion of the ring being driven normal between each pair so as to obtain data similar to that in Fig. 1, but at a fixed frequency (± 1 mHz). The rotor frequency was then changed as quickly as possible to ν_2 and the measurement sequence performed in reverse, i.e., first with the ring superconducting and then normal. The value of δ was obtained from the two "*N*" data sets and the corresponding $\Delta\nu(\delta)$ from the two included "*S*" sets. During the change from ν_1 to ν_2, the *same* small portion of the ring was driven normal periodically to keep the current in the ring close to zero, and no data were recorded. The fact that the flux nulls between ν_1

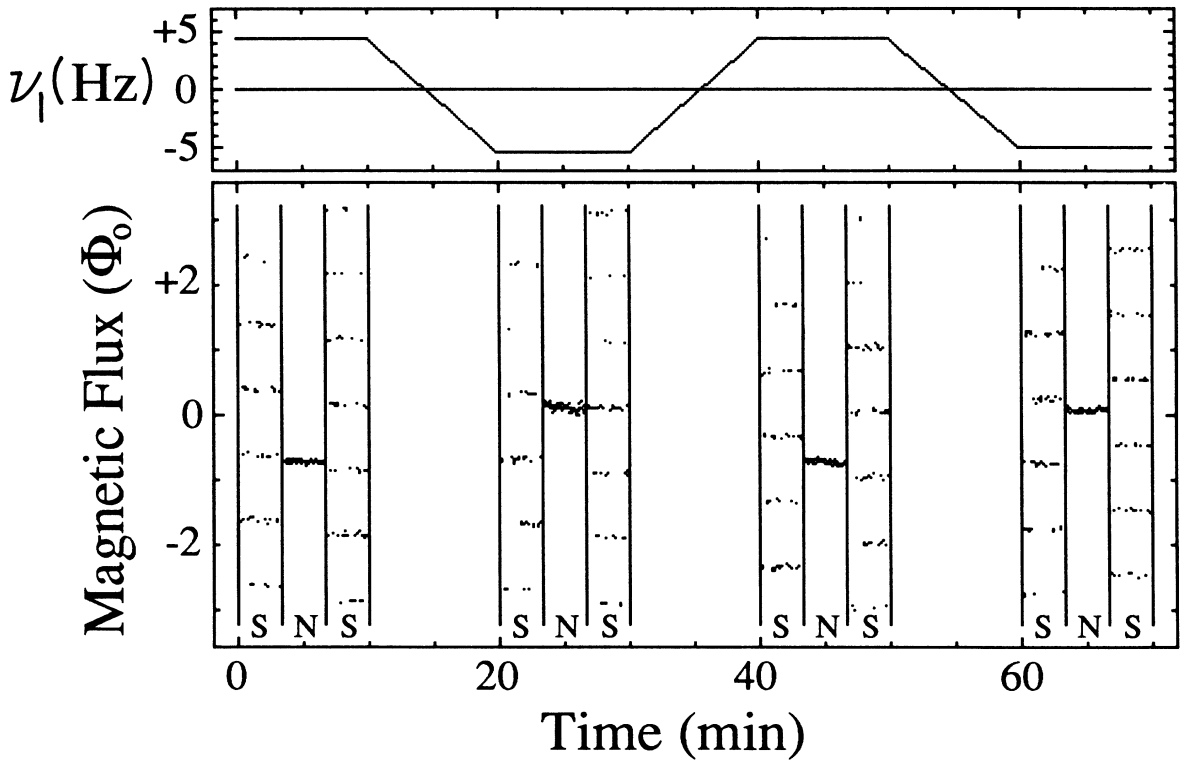

FIG. 5. Data acquisition scheme. The upper box shows the rotor spin frequency and the lower box the corresponding flux measured by the magnetometer. When the ring is superconducting (*S*), the flux is quantized, and when it is normal (*N*) the flux has a single value.

and ν_2 went unrecorded was of no consequence because preliminary measurements at intermediate, incommensurately spaced, frequencies gave a value of $\Delta\nu$ with sufficient accuracy to determine exactly the integer number of unrecorded nulls.

It took about 5 s to record each flux-frequency pair, and an average of 2 min/Hz to change the rotor frequency, including stabilizing the temperature of the gas flow at the new frequency. The end frequencies of the range were sometimes of opposite sign, and sometimes not, in order to reveal any asymmetry in the rotor's operation in the clockwise (cw) and counterclockwise (ccw) directions. Typical frequency ranges were 2 and 8 Hz. In effect, this was a low-frequency ac measurement with a period of order 20 min. In principle, the larger the frequency range, the greater the accuracy of $\Delta\nu$, because of the greater number of nulls spanned. In practice, a larger frequency range also meant a longer time between the two measurements and increased problems with SQUID drift. Also, the rotor's performance at higher rotation rates (>5 Hz) was less reliable.

Usually, about 10 $(\delta, \Delta\nu(\delta))$ points were recorded in a 1-d run, and many such sets were recorded. The experiment was removed from the cryostat every few months, various changes implemented, and then run once again. Most of the data presented below were taken during the course of a year, but data from the previous two years of operation show remarkable consistency.

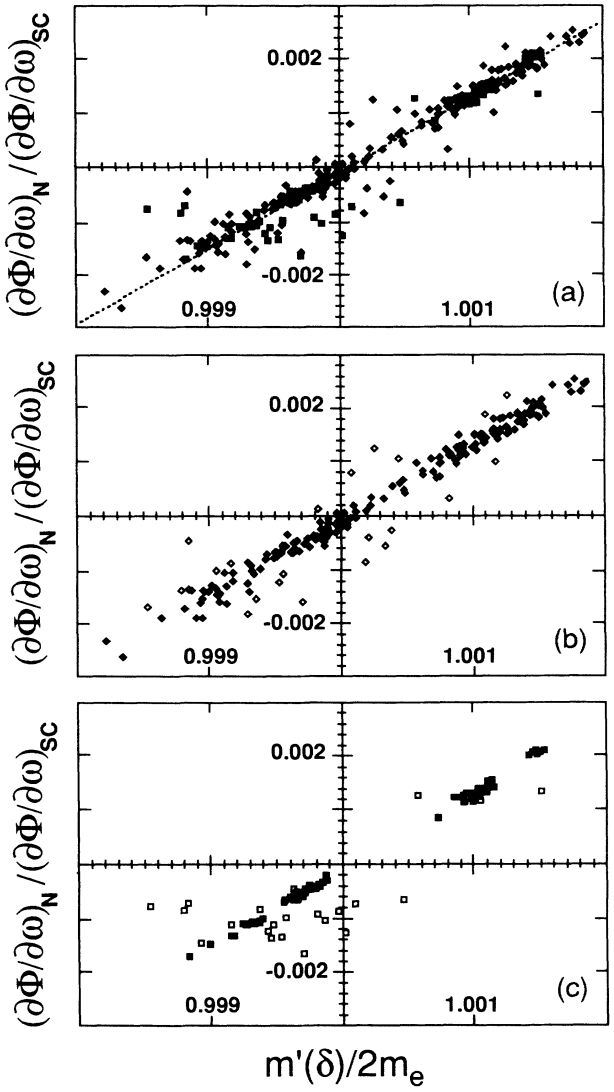

FIG. 6. (a) Plot of $\delta \equiv (\partial\phi/\partial\omega)_N/(\partial\phi\partial\omega)_{SC}$ vs $m'(\delta)/2m_e$ showing 310 points. Diamonds represent the 202 points obtained from a 2-Hz interval and squares the 108 points from an 8-Hz interval. The dotted line corresponds to $\epsilon = 0.705$ and $m'(0)/2m_e = 1.000\,084$. (b) Same as (a) for ~2-Hz data only. Open symbols show points that were discarded in the cut. (c) Same as (a) for ~8-Hz data only. Open symbols show points that were discarded in the cut.

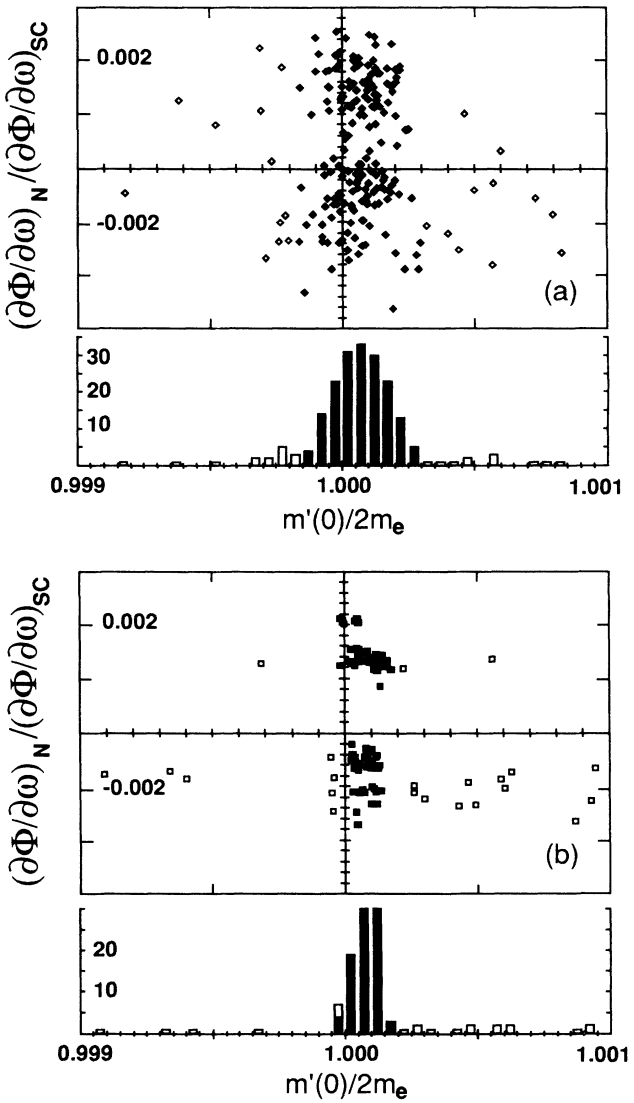

FIG. 7. Plot of $\delta \equiv (\partial\phi/\partial\omega)_N/(\partial\phi\partial\omega)_{SC}$ vs $m'(0)/2m_e$ obtained from each point by translation along the line corresponding to $\epsilon = 0.705$. Open symbols show points that were discarded in the cutting procedure. The bar graph below the plot shows the distribution for all data points (open bars) and for the subset that survived the cut (solid bars). (a) Data from an ~2-Hz interval. (b) Data from an ~8-Hz interval.

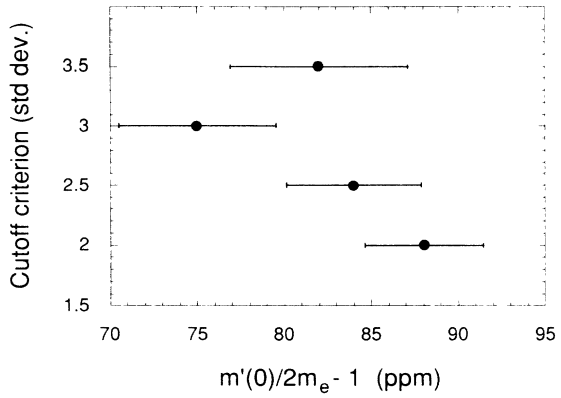

FIG. 8. Effect of altering the cutoff criterion in the analysis procedure.

IV. RESULTS

Each point in the S data sets in Fig. 5 was assigned (without error) its quantum state n and the corresponding flux null ν_n was calculated from the predetermined London moment slope (approximately 70 ϕ_0/Hz for our geometry). The flux null spacing $\Delta\nu$ was computed from the slope of the line relating ν_n to n. The statistical error in $\Delta\nu$ was typically 10 ppm for a frequency range $(\nu_2-\nu_1)$ of 8 Hz. Since about 560 flux nulls were spanned, this implies that each ν_n was determined to about 0.4%. The corresponding value of δ was obtained from the data taken with the ring normal. In Fig. 5, for example, the value of $(\partial\phi/\partial\omega)_N$ is $\sim 0.1\phi_0$/Hz, or $\delta\sim 10^{-3}$. Note that the data determining δ bracket those which determine $\Delta\nu$. The results are plotted in Fig. 6, which show δ as the y axis and the measured value of $m'(\delta)/2m_e$ (inversely proportional to $\Delta\nu$) as the x axis. The linear relationship predicted by Eq. (8) is verified and the slope of the line through the points agrees well with the calculated value of $\epsilon=0.7$. The 310 data points presented in Fig. 6 were taken during a set of runs carefully designed to test many sources of systematic error. What is remarkable is that 630 data points were taken during different runs over a period of some 3 yr (including those presented in Ref. 5), with various changes implemented from time to time, all fall close to the same straight line.

The extraction of the value of $m'/2m_e$ at $\delta=0$ was complicated by the presence of the outlying data points evident in Fig. 6(a). Most of the points form a Gaussian distribution about the best-fit line, with the remaining 15% of the points distributed in a nonstatistical fashion. One explanation for the existence of these outliers is that a flux vortex became trapped in the niobium film during the time that the flux was not recorded. This results in an offset between the flux measured (when the ring is superconducting) at ν_1 with respect to that at ν_2 by some unknown amount, and a large error in $\Delta\nu$ (up to 900 ppm at $\nu_1-\nu_2=8$ Hz and larger for smaller-frequency ranges).

The procedure adopted to extract a sensible value for $m'(0)$ is known as Chauvenet's criterion,[17] which, for a single variable, involves computing the mean and standard deviation of all data, including outliers, then discarding data points which lie more than 2.5 standard deviations from the mean. A new mean and standard deviation are calculated with the remaining points, and the procedure repeated until no more points are discarded. In our case, with two correlated variables, we adjust the procedure slightly. The slope of the least-squares straight line through all the data is found, and each point translated to the $\delta=0$ axis along a line with such a slope. The problem is then the same as for the single variable case, and outliers are discarded according to the criterion. The least-squares straight line for the remaining points is calculated, and the points translated to the $\delta=0$ axis with the new slope, and so on. For the data shown in Fig. 6(a), five such iterations were necessary, and 45 points were discarded. The δ intercept and slope, with their corresponding error estimates, for the least-squares line in the final iteration gave $m'(0)/2m_e$ and ϵ with statistical errors

$$m'(0)/2m_e=1.000\,084(5)$$

and

$$\epsilon=0.705(7)\ .$$

Figure 6(a) shows all the points included in this analysis with a dotted line superimposed corresponding to the parameters obtained in the final iteration. Figures 6(b) and 6(c) show the data in 6(a) divided into points obtained from ~ 2 and ~ 8-Hz intervals, respectively. Open symbols represent points removed in the cut. Figures 7(a) and 7(b) present the data in 6(b) and 6(c), respectively, in a different way. Using the best-fit parameters, a value of $m'(0)$ is obtained from each measured value for $m'(\delta)$, and is plotted against δ in the upper part of each figure. The lower part is a histogram which counts the number of points in each 50-ppm range of $m'(0)$. The solid portion of the bar represents the points that survived the cut, with a cutoff criterion of 2.5 standard deviations in this case. The effect of varying this criterion is displayed in Fig. 8.

To make certain that the analysis did not bias the results, subsets of the data were analyzed separately. Those data obtained from an 8-Hz frequency change [~ 560 nulls, Figs. 6(c), and 7(b)] were analyzed separately from those obtained from a 2-Hz change [~ 140 nulls, Figs. 6(b) and 7(a)]. The spread in the data was narrower for the data taken over an 8-Hz range, as expected. Also, data were divided into smaller groups according to other criteria, e.g., whether the two end frequencies used were both clockwise, both counterclockwise, or one of each. No clear evidence of systematic error from such sources was found.

Even if the rotor had not been not charged, a similar effect would have been present at a lower level because quartz has a finite magnetic susceptibility, and, when set into rotation, becomes uniformly magnetized. This magnetization is known as the Barnett moment[18] and is $\mathbf{M}=\chi_m(2m_ec/e)\omega$ if the magnetization is produced by electron orbital moments and $\mathbf{M}=\chi_m(m_ec/e)\omega$ if it is produced by electron-spin moments. The resultant mag-

TABLE I. Error budget for the determination of m'.

Flux null spacing determination	
Statistical fit for rotation-dependent moments ($e=0.70$)	± 5
Nonuniform charge distribution	± 5
SQUID drift ($\epsilon=1$)	± 2
Rotor position shift in housing	± 16
Frequency counter	± 0.1
Misalignment of area and spin vectors	± 1
Area determination and fundamental constants	
$S=20.235\,057(179)$ cm^2	± 8.86
$h=6.626\,0755(40)\times 10^{-34}$ J s	± 0.6
$m_e=9.109\,3897(54)\times 10^{-31}$ kg	± 0.59
Cooper-pair mass	
$[m'/(2m_e)]_{\mathrm{Nb}}=1.000\,084$	± 21

netic field inside the quartz has the same sign as the London moment ($\chi_m<0$ as quartz is diamagnetic and $e<0$ since the charges responsible for the diamagnetism are electrons) and is smaller by a factor of $4\pi\chi_m$. Since a uniform magnetization is mathematically equivalent to a surface current distribution, the Barnett moment couples to the supercurrents in the ring and SQUID pickup loop in exactly the same way as the electrostatic charge ($\epsilon=0.7$). From the value of χ_m for quartz,[19] we deduce a value of δ of about 1×10^{-5}, so even in the absence of a rotor charge, we would expect our measured value of m' to be shifted by 7 ppm. The effect of the Barnett moment is accounted for in the fitting procedure described above.

The flux at the SQUID can change as the rotor spins for reasons unrelated to charge- or rotation-dependent moments. The SQUID itself has a $1/f$ noise spectrum below a knee frequency of about 0.1 Hz, and exhibits white noise above. Since one measurement of δ and $\Delta\nu(\delta)$ took up to 20 min, we are firmly in the $1/f$ region. We modeled the effect of the $1/f$ noise on the measurement of $\Delta\nu$ using a computer-generated $1/f$ noise spectrum to simulate the SQUID output, and found that variations in δ and $\Delta\nu(\delta)$ of order 200 ppm are to be expected on top of the actual variations in the charge. Thus, while the large-scale variation in δ (some 4000 ppm over a period of months) was due to real change in the amount of charge on the rotor, short-term variations on the order of 100 ppm were probably due to SQUID $1/f$ noise. Temperature changes also caused the output of the SQUID to change by about 0.004 ϕ_0/mK, so the temperature of the bearing exhaust gas, as recorded by a germanium resistance thermometer (GRT), was measured after each set of 70 data pairs. There were heaters in the gas lines, as part of a feedback loop which also included the GRT, to regulate the temperature of the exhaust gas, but the temperature tended to stabilize at different values for the same control parameter, depending on the gas flow. The maximum temperature shift was about 2–3 mK for a frequency range of 8 Hz and less than 1 mK for a range of 2 Hz. The effect on this type of drift on the flux null spacing is similar to that described by Eq. (7), only with $\epsilon=1$, because there is no coupling to the supercurrent in the ring. Since we estimate that the magnitude of the shifts in $m'/2m_e$ due to drift to be in the region 10^{-5} to 10^{-4}, while shifts due to the charge can range up to $\pm 2\times 10^{-3}$, we expect that the effect of the drift is to broaden the distribution of points around the straight line with a slope of 0.7. If the distribution of charge on the rotor changes in shape as well as magnitude, we also expect a broadening of the distribution of points because of the differing values of ϵ near 0.7. We estimate that the maximum uncertainty in $m'(0)/2m_e$ introduced by this broadening is 7 ppm.

The SQUID was also sensitive to changes of the rotor position in the housing when the ring was superconducting, because the effective mutual inductance between the ring and SQUID pickup loop changed, and because of the magnetic field gradient at the ring generated by the current in the pickup loop. Thermal gradients generated large currents in the pickup loop as it cooled from its superconducting transition temperature to 6 K. Rather drastic changes in the gas flows to the top and bottom bearings of the housing caused an offset at the SQUID which corresponded to about 1 ϕ_0 at the ring. It proved possible to null the effects of the thermal gradients by trapping a suitable field in the pickup loop as it went through its superconducting transition. The sensitivity to the rotor position was thereby reduced to less than 0.05 ϕ_0 at the ring. Also, the changes in gas flow during the experiment were not nearly as extreme as those used to test this sensitivity, so we conservatively estimate a 0.01-ϕ_0 residual effect. This introduces an uncertainty of about 16 ppm in our determination of the flux null spacing. This source of error is not accounted for by our linear fitting procedure because the SQUID is insensitive to changes in the rotor position when the ring is normal.

An error budget is presented in Table I. In addition to the error sources discussed above, we include the error in the frequency counter (0.1 ppm), misalignment of the rotor spin axis and area vector (1 ppm), and the errors in

the fundamental constants used to calculate the final results.[20] The errors from systematic effects we estimate at 21 ppm, and thus our final result is

$$(m'/2m_e)_{\mathrm{Nb}} = 1.000\,084(21)\ ,$$

where the statistical and systematic errors have been combined as the root sum of squares.

V. DISCUSSION

The result disagrees with the theories presented in Sec. II and, in fact, lies almost halfway between the predicted values of the observable mass m' and the intrinsic mass m^* and ~ 5 standard deviations from each. Much of the scatter in the data from this experiment can be attributed to the SQUID magnetometer whose noise spectrum is $1/f$ below 100 mHz, and white above. A SQUID with a knee frequency in the mHz region would significantly reduce the spread. A scheme to switch the SQUID input circuit at high frequency is presently being developed to overcome this problem.[21] The area determination could be fairly readily improved to ppm accuracy.[12] The effect of the charge on the rotor could be somewhat reduced in a setup where two superconducting rings of different materials were deposited close together, one on either side of the rotor equator so that their areas were equal. A differential measurement of the masses would then be possible at a single frequency by determining whether the flux nulls for the different rings are coincident.

ACKNOWLEDGMENTS

This work was funded by the National Science Foundation under Grant Nos. DMR-80-26007 and DMR-84-05384 and by the National Bureau of Standards under Grant No. G8-9026. We thank John T. Anderson for the design of much of the electronics and for valuable discussions. The area measurement was performed in collaboration with David McIntyre, and we thank Professor Arthur Schawlow for the loan of the laser and computing facilities. Technical assistance from W. Jung and L. Goddard is gratefully acknowledged.

---

*Present address: Department of Physics, Oregon State University, Corvallis, OR 97331-6507.

†Present address: Varian Research Center, 611 Hansen Way, Palo Alto, CA 94303.

[1]F. H. London, *Superfluids* (Wiley, New York, 1950), Vol. 1.

[2]A. F. Hildebrandt, Phys. Rev. Lett. **12**, 190 (1964).

[3]J. E. Zimmerman and J. E. Mercereau, Phys. Rev. Lett. **12**, 887 (1965).

[4]W. H. Parker and M. B. Simmonds, Natl. Bur. Stand. (U.S.) Spec. Publ. No. 343 (U.S. GPO, Washington, D.C., 1970).

[5]S. B. Felch, J. Tate, B. Cabrera, and J. T. Anderson, Phys. Rev. B **31**, 7006 (1985); S. B. Felch, Ph.D. thesis, Stanford University, 1984.

[6]J. Tate, B. Cabrera, S. B. Felch, and J. T. Anderson, Phys. Rev. Lett. **62**, 845 (1989). The equation in the abstract of this Letter should read $\hbar/m' = 25\Delta v$.

[7]P. W. Anderson, in *Progress in Low Temperature Physics*, edited by C. J. Gorter (North-Holland, Amsterdam, 1967), Vol. 5.

[8]R. M. Brady, J. Low. Temp. Phys. **49**, 1 (1982).

[9]B. Cabrera, H. Gutfreund, and W. A. Little, Phys. Rev. B **25**, 6644 (1982).

[10]J. Anandan, Phys. Lett. **105A**, 280 (1984); J. Anandan, Ann. N.Y. Acad. Sci. **480**, 224 (1986).

[11]B. Cabrera and M. Peskin, Phys. Rev. B **39**, 6425 (1989).

[12]J. Tate, D. H. McIntyre, and B. Cabrera, Rev. Sci. Instrum. **60**, 985 (1989).

[13]B. Cabrera and G. J. Siddall, Precis. Eng. **3**, 125 (1981).

[14]B. Cabrera and F. van Kann, Acta Astron. **5**, 125 (1978).

[15]S. A. Wolf, J. J. Kennedy, and M. Nisenoff, J. Vac. Sci. Tech. **13**, 145 (1976).

[16]J. Tate, Ph.D. thesis, Stanford University, 1987.

[17]H. D. Young, *Statistical Treatment of Experimental Data* (McGraw-Hill, New York, 1962), pp. 78–80.

[18]See, for example, L. F. Bates, *Modern Magnetism*, 4th ed. (Cambridge University Press, London, 1961), p. 243.

[19]$\chi_m = (B + C/T)\rho$ with $B = -0.383 \times 10^{-6}$ cm^3/g, $C = +0.005 \times 10^{-6}$ cm^{3}K/g, $\rho = 2.2$ g/cm^3 [R. L. Fagaly (private communication), measured with S. H. E. Model VTS-905 SQUID Susceptometer)].

[20]E. R. Cohen and B. N. Taylor, J. Res. Natl. Bur. Stand. **92**, 85 (1987).

[21]J. T. Anderson, B. Cabrera, M. A. Taber, S. B. Felch, and J. Tate, Rev. Sci. Instrum. **60**, 202 (1989); J. T. Anderson, B. Cabrera, and M. A. Taber, *ibid.* **60**, 209 (1989).

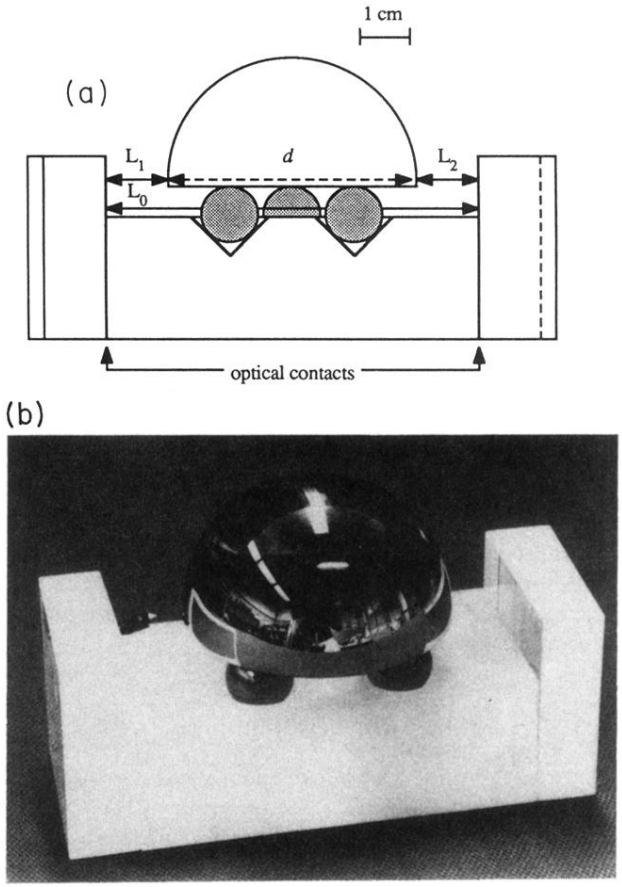

FIG. 2. (a) Schematic of the rotor in the optically contacted Fabry-Perot etalon used for the diameter determination. (b) Photograph of the apparatus.

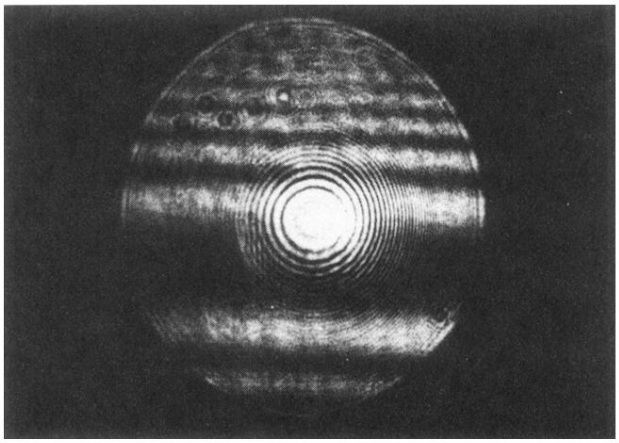

FIG. 3. Circular interference pattern produced by the laser light in one of the optical cavities in Fig. 2. The superimposed parallel line diffraction pattern is from the niobium ring.

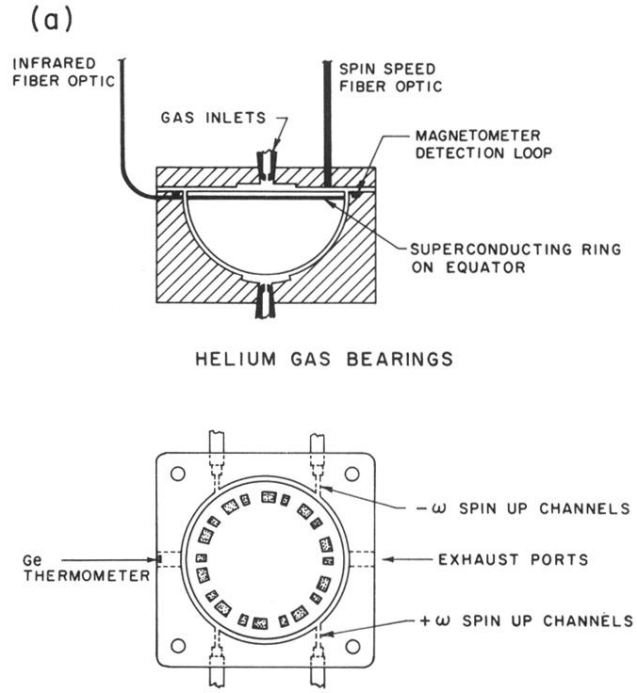

FIG. 4. (a) Schematic of the fused quartz apparatus used to determine flux null spacing. (b) Photograph of the apparatus.